

Fracture analysis of inhomogeneous arch with two longitudinal cracks under non-linear creep

Victor I. Rizov*¹ and Holm Altenbach²

¹Department of Technical Mechanics, University of Architecture, Civil Engineering and Geodesy,
Chr. Smimensky Blvd., 1046-Sofia, Bulgaria

²Lehrstuhl für Technische Mechanik, Fakultät für Maschinenbau, Otto-von-Guericke-Universität Magdeburg,
Universitätsplatz 2, 39106 Magdeburg, Deutschland

(Received February 23, 2022, Revised April 21, 2022, Accepted April 28, 2022)

Abstract. In this paper, fracture analysis of a continuously inhomogeneous arch structure with two longitudinal cracks is developed in terms of the time-dependent strain energy release rate. The arch under consideration exhibits non-linear creep behavior. The cross-section of the arch is a rectangle. The material is continuously inhomogeneous along the thickness of the cross-section. The arch is loaded by two bending moments applied at its end sections. The mechanical behavior of the material is described by using a non-linear stress-strain-time relationship. The two longitudinal cracks are located symmetrically with respect to the mid-span of the arch. Due to the symmetry, only half of the arch is considered. Time-dependent solutions to strain energy release rate are obtained by analyzing the balance of the energy. For verification, time-dependent solutions to the strain energy release rate are derived also by considering the time-dependent complementary strain energy. The evolution of the strain energy release rate with the time is analyzed. The effects of material inhomogeneity, locations of the two cracks along the thickness of the arch and the magnitude of the external loading on the time-dependent strain energy release rate are evaluated.

Keywords: analytical investigation; inhomogeneous arch; longitudinal crack; non-linear creep behavior; time-dependent solution

1. Introduction

The advance in current engineering requires development and application of new materials. In particular, the continuously inhomogeneous structural materials whose properties are smooth functions of the coordinates are more efficacious in comparison to the conventional homogeneous materials. Very advantageous kind of continuously inhomogeneous materials are the functionally graded materials which have attracted significant attention as advanced structural materials in various engineering applications in the recent decades (Altunsaray and Bayer 2014, Altunsaray 2017, Altunsaray *et al.* 2019, Avcar and Mohammed 2018, Butcher *et al.* 1999, Gasik 2010, Hedia *et al.* 2014). The functionally graded materials are continuously inhomogeneous composites which

*Corresponding author, Professor, E-mail: V_RIZOV_FHE@UACG.BG

^aProfessor, E-mail: holm.altenbach@ovgu.de

are made of two or more constituent materials. One of the fundamental advantages of this kind of materials over the homogeneous materials is the fact that the properties of functionally graded materials can be formed by gradually varying the composition of the constituent materials along one or more directions in the solid during manufacturing (Hirai and Chen 1999, Kashinath Saha and Shubhankar Bhowmick 2020, Mahamood and Akinlabi 2017, Markworth *et al.* 1995, Miyamoto *et al.* 1999, Nemat-Allal *et al.* 2011, Rabenda 2015, Rabenda and Michalak 2015, Rabenda, 2016, Ridha *et al.* 2016, Saiyathibrahim *et al.* 2016). In this way, different performance requirements in different parts of a structural member can be satisfied. Therefore, functionally graded materials have been widely used for manufacturing of various sophisticated devices and structures in aeronautics, nuclear reactors, electronics, biomedicine, robotics and optics (Shrikantha Rao and Gangadharan 2014, Sofiyev and Avcar 2010, Sofiyev *et al.* 2012, Uslu Uysal and Kremzer 2015, Uslu Uysal 2016, Uslu Uysal and Güven 2015, Wu *et al.* 2014).

The integrity of structures made of continuously inhomogeneous materials depends in high degree of their fracture behavior. Therefore, considerable attention has been paid to the problems of fracture of continuously inhomogeneous (functionally graded) materials and structures by the international research community in the recent years (Dolgov 2005, Dolgov 2016, Uslu Uysal and Güven 2016).

Certain kinds of continuously inhomogeneous materials, such as the functionally graded materials, can be built-up layer-by-layer (Mahamood and Akinlabi 2017) which is a premise for appearance of longitudinal cracks between layers. Therefore, an adequate longitudinal fracture analysis of continuously inhomogeneous structural members and components is very important for evaluation of their operational performance. Recently, several papers which are focused on longitudinal fracture of continuously inhomogeneous beams have been published (Rizov 2020, Rizov 2020a, Rizov and Altenbach 2020, Rizov 2022).

The present paper aims to develop a fracture analysis of a continuously inhomogeneous arch structure with two longitudinal cracks in contrast to (Rizov 2020, Rizov 2020a) where beam structures are analyzed. The originality of the present paper consists also in the fact that the arch under consideration exhibits non-linear creep behavior in contrast to (Rizov 2022) where fracture in beams is analyzed assuming linear creep behavior. The longitudinal fracture in the arch is studied in terms of the strain energy release rate. In order to take into account the non-linear creep behavior, time-dependent solutions to the strain energy release rate are derived. It should also be mentioned that the two cracks are located inside the arch structure in contrast to (Rizov 2020, Rizov 2020a, Rizov 2022) where the crack is located at the edge of the beam. Since the two cracks are inside the arch, the bending moments which are used to derive time-dependent solutions to the strain energy release rate are determined by analyzing the arch as a statically undetermined structure with one internal hyperstatic unknown.

2. Inhomogeneous arch structure with two longitudinal cracks under non-linear creep

The inhomogeneous half-sine slender arch with small initial curvature shown in Fig. 1 is under consideration. The cross-section of the arch is a rectangle of width, b , and thickness, h . Two longitudinal cracks, B_1B_2 and C_1C_2 , are located symmetrically with respect to the mid-span of the arch as shown in Fig. 1. The lengths of cracks, B_1B_2 and C_1C_2 , are denoted by $2a_1$ and $2a_2$, respectively. In portion, D_2D_3 , the arch is divided by the two cracks in inner, middle and outer parts

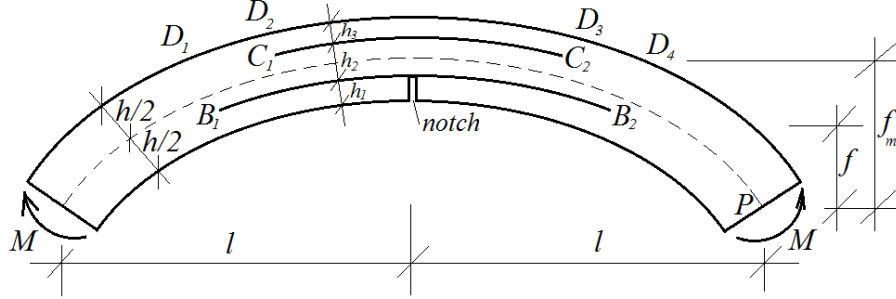


Fig. 1 Geometry and loading of an inhomogeneous arch structure with two longitudinal cracks

of thicknesses, h_1 , h_2 and h_3 , respectively. In portions, D_1D_2 and D_3D_4 , the arch is divided by crack, B_1B_2 , in inner and outer parts of thicknesses, h_1 and $h_2 + h_3$, respectively. The external loading consists of two bending moments, M , applied at the ends of the arch.

A notch of depth, h_1 , is cut-out in the inner part of the arch as shown in Fig. 1. Due to the notch, the inner part of the arch in portion, $D_1 \rightarrow D_4$, is free of stresses. The initial shape of the arch is written as (Fig. 1)

$$f = f_m \sin \beta, \quad (1)$$

where

$$0 \leq \beta \leq \pi. \quad (2)$$

In formula (1), f_m is the rise of the arch.

The arch exhibits non-linear creep. Therefore, the mechanical behavior of the material is treated by using the following non-linear stress-strain-time-relationship (Kishkilov and Apostolov, 1994):

$$\varepsilon = \frac{\sigma}{E} + L\sigma^n \frac{t}{1 + H^q t^q}, \quad (3)$$

where ε is the strain, σ is the stress, E is the modulus of elasticity, n , L , q and H are material parameters, t is time. The material of the arch is continuously inhomogeneous in the thickness direction. Therefore, the continuous distribution of the modulus of elasticity along the thickness of the arch is expressed as

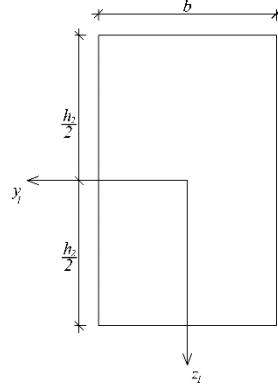
$$E = E_F e^{\frac{g}{h} \left(\frac{h}{2} + z \right)}, \quad (4)$$

where

$$-\frac{h}{2} \leq z \leq \frac{h}{2}. \quad (5)$$

In formula (4), E_F is the value of the modulus of elasticity in the outer surface of the arch, g is a material parameter that controls the material inhomogeneity in the thickness direction, z is the vertical centroidal axis of the cross-section.

In the present paper, time-dependent solutions to the strain energy release rate, G , are derived by considering the balance of the energy. Only the right-hand half of the arch is analyzed due to

Fig. 2 Cross-section of the middle part of portion, D_2D_3 , of the arch

the symmetry. First, a time-dependent solution to the strain energy release rate is derived assuming a small increase, δa_1 , of the length of crack, B_1B_2 . For this purpose, the balance of the energy is written as

$$M\delta\phi = \frac{\partial U}{\partial a_1} \delta a_1 + Gb\delta a_1, \quad (6)$$

where ϕ is the angle of rotation of the end section of the arch, U is the strain energy cumulated in half of the arch. Form (6), G is expressed as

$$G = 2 \left(\frac{M}{b} \frac{\partial \phi}{\partial a_1} - \frac{1}{b} \frac{\partial U}{\partial a_1} \right). \quad (7)$$

The expression in the brackets in (7) is doubled in view of the symmetry (Fig. 1).

The angle of rotation of the end section of the arch is obtained by applying the integrals of Maxwell-Mohr

$$\phi = \int_0^{a_2} \kappa_1 ds + \int_{a_2}^{a_1} \kappa_2 ds + \int_{a_1}^{s_l} \kappa_3 ds, \quad (8)$$

where κ_1 , κ_2 and κ_3 are, respectively, the changes in the curvatures of the middle part of portion, D_2D_3 , of the arch, of the outer part of portion, D_3D_4 , of the arch and of the un-cracked portion, B_2P , of the arch, s_l is half length of the arch.

The change of the curvature, κ_1 , is determined in the following way. First, the equations for equilibrium of the cross-section of the middle part of portion, D_2D_3 , of the arch are written as

$$N_1 = \iint_{(A_1)} \sigma dA, \quad (9)$$

$$M_1 = \iint_{(A_1)} \sigma z_1 dA, \quad (10)$$

where N_1 and M_1 are the axial force and the bending moment (it is obvious that $N_1 = 0$), σ is the normal stress, z_1 is the vertical centroidal axis, A_1 is area of the cross-section of the middle part of

portion, D_2D_3 , of the arch (Fig. 2). The stress, σ , has to be expressed in a function of z_1 in order to perform the integration in (9) and (10). However, the normal stress can not be obtained explicitly from (3). Therefore, σ is expanded in series of Maclaurin by retaining the first three members

$$\sigma(z_1) \approx \sigma(0) + \frac{\sigma'(0)}{1!} z_1 + \frac{\sigma''(0)}{2!} z_1^2. \quad (11)$$

Expression (11) is rewritten as

$$\sigma(z_1) \approx \delta + \phi z_1 + \eta z_1^2. \quad (12)$$

The coefficients, δ , ϕ and η , involved in (12) are determined in the following way. First, the distribution of the strain, ε , that is involved in (3) is written as

$$\varepsilon = \varepsilon_{ct} + \kappa_1 z_1, \quad (13)$$

where ε_{ct} is the strain in the centre of the cross-section of the middle part of portion, D_2D_3 , of the arch. It should be noted that formula (19) is based on the assumption that plane cross-sections remain plane after deformation since the arch is thin (the thickness of the arch is much smaller than the radius). By using (4), the distribution of the modulus of elasticity in the middle part of the arch is expressed as

$$E = E_F e^{\frac{g}{h} \left(h - h_1 - \frac{h_2}{2} + z_1 \right)}, \quad (14)$$

where

$$-\frac{h_2}{2} \leq z_1 \leq \frac{h_2}{2}. \quad (15)$$

By substituting of (12), (13) and (14) in (3), one obtains

$$\varepsilon_{ct} + \kappa_1 z_1 = \frac{\delta + \phi z_1 + \eta z_1^2}{E_F e^{\frac{g}{h} \left(h - h_1 - \frac{h_2}{2} + z_1 \right)}} + \left(\delta + \phi z_1 + \eta z_1^2 \right)^n \frac{Lt}{1 + H^q t^q}. \quad (16)$$

At $z_1 = 0$ equation (16) takes the form

$$\varepsilon_{ct} = \frac{\delta}{E_F e^{\frac{g}{h} \left(h - h_1 - \frac{h_2}{2} \right)}} + \delta^n \frac{Lt}{1 + H^q t^q}. \quad (17)$$

By substituting of $z_1 = 0$ in the first and the second derivatives of (16) with respect to z_1 , one obtains

$$\kappa_1 = \frac{\phi - \frac{\delta g}{h}}{E_F e^{\frac{gm}{h}}} + n \delta^{n-1} \phi \frac{Lt}{1 + H^q t^q}, \quad (18)$$

$$0 = \frac{2\eta - 2\phi \frac{g}{h} + \delta \frac{g^2}{h^2}}{E_F e^{\frac{gm}{h}}} + \left[(n-1) \delta^{n-2} \phi^2 + 2\delta^{n-1} \eta \right] \frac{nLt}{1 + H^q t^q}, \quad (19)$$

where $m = h - h_1 - h_2/2$. After substitution of (12) in (9) and (10), one arrives at

$$N_1 = \delta b h_2 + \frac{1}{12} \eta b h_2^3, \quad (20)$$

$$M_1 = \frac{1}{12} \phi b h_2^3. \quad (21)$$

There are six unknowns, M_1 , κ_1 , ε_{ct} , δ , ϕ and η , in Eqs. (17)-(21).

Analogically, five equations are obtained by expanding in series of Maclaurin the normal stress, σ_{ou} , in the outer part of portion, D_2D_3 , of the arch and by using the equations for equilibrium of the cross-section of the outer part

$$\varepsilon_{ctou} = \frac{\delta_{ou}}{E_F e^{\frac{gh_3}{2h}}} + \delta_{ou}^n \frac{Lt}{1 + H^q t^q}, \quad (22)$$

$$\kappa_4 = \frac{\phi_{ou} - \frac{\delta_{ou} g}{h}}{E_F e^{\frac{gh_3}{2h}}} + n \delta_{ou}^{n-1} \phi_{ou} \frac{Lt}{1 + H^q t^q}, \quad (23)$$

$$0 = \frac{2\eta_{ou} - 2\phi_{ou} \frac{g}{h} + \delta_{ou} \frac{g^2}{h^2}}{E_F e^{\frac{gh_3}{2h}}} + [(n-1) \delta_{ou}^{n-2} \phi_{ou}^2 + 2\delta_{ou}^{n-1} \eta_{ou}] \frac{nLt}{1 + H^q t^q}, \quad (24)$$

$$N_2 = \delta_{ou} b h_3 + \frac{1}{12} \eta_{ou} b h_3^3, \quad (25)$$

$$M_2 = \frac{1}{12} \phi_{ou} b h_3^3, \quad (26)$$

where ε_{ctou} is the strain in the centre of the cross-section of outer part of portion, D_2D_3 , of the arch, κ_4 is the change of the curvature, N_2 and M_2 are, respectively, the axial force and the bending moment (apparently, $N_2 = 0$), δ_{ou} , ϕ_{ou} and η_{ou} are the coefficients in the series of Maclaurin.

One equation is written by considering the equilibrium of the bending moments in the middle and outer parts of portion, D_2D_3 , of the arch

$$M_1 + M_2 = M. \quad (27)$$

It should be noted here that the bending moment in the inner part of the portion, D_1D_4 , of the arch is zero due to the notch.

Further one equation is composed by treating the arch as a structure with one degree of internal static indeterminacy (the bending moment in the outer part of portion, D_2D_3 , of the arch is taken as hyperstatic unknown). The static indeterminacy is resolved by applying the theorem of Castigliano for structures which exhibit non-linear mechanical behavior of the material

$$\frac{\partial U^*}{\partial M_2} = 0, \quad (28)$$

where the complementary strain energy, U^* , is found as

$$U^* = U_{md}^* + U_{ou}^* + U_{ou34}^*. \quad (29)$$

In formula (29), U_{md}^* , U_{ou}^* and U_{ou34}^* are the complementary strain energies cumulated in the middle and in the outer parts of portion, D_2D_3 , of the arch and in the outer part of portion, D_3D_4 , of the arch, respectively. It should be noted that that the complementary strain energy cumulated in the un-cracked portion, B_2P , of the arch does not depend M_2 . Therefore, the complementary strain energy in the un-cracked portion of the arch is not involved in (29).

The complementary strain energy cumulated in half of the middle part of portion, D_2D_3 , of the arch is expressed as

$$U_{md}^* = a_2 \iint_{(A_1)} u_{0md}^* dA \quad (30)$$

where u_{0md}^* is the complementary strain energy density. In principle, the complementary strain energy density is equal to the area that supplements the area enclosed by the stress-strain curve to a rectangle. Thus, u_{0md}^* is written as

$$u_{0md}^* = \sigma \varepsilon - u_{0md}, \quad (31)$$

where the strain energy density, u_{0md} , is equal to the area enclosed by the stress-strain curve

$$u_{0md} = \int_0^\varepsilon \sigma d\varepsilon. \quad (32)$$

By combining of (3), (31) and (32), one derives the following expressions for the time-dependent strain energy and complementary strain energy densities

$$u_{0md} = \frac{\sigma^2}{2E} + \frac{n}{n+1} \sigma^{n+1} \frac{Lt}{1+H^q t^q}, \quad (33)$$

$$u_{0md}^* = \frac{\sigma^2}{2E} + \frac{1}{n+1} \sigma^{n+1} \frac{Lt}{1+H^q t^q}. \quad (34)$$

The complementary strain energy in the outer part of portion, D_2D_3 , of the arch, u_{0ou}^* , is obtained by replacing of σ with σ_{ou} in (34). The complementary strain energy density, u_{0ou34}^* , in the outer part of portion, D_3D_4 , of the arch is calculated by replacing of σ with σ_{ou34} in (34). The normal stress, σ_{ou34} , in the outer part of portion, D_3D_4 , of the arch is expanded in series of Maclaurin. The coefficients of the series are determined by using the following equations

$$\varepsilon_{ctou34} = \frac{\delta_{ou34}}{E_F e^{\frac{g}{h} \left(\frac{h_2}{2}, \frac{h_3}{2} \right)}} + \delta_{ou34}^n \frac{Lt}{1+H^q t^q}, \quad (35)$$

$$\kappa_2 = \frac{\phi_{ou34} - \frac{\delta_{ou34} g}{h}}{E_F e^{\frac{g}{h} \left(\frac{h_2}{2}, \frac{h_3}{2} \right)}} + n \delta_{ou34}^{n-1} \phi_{ou34} \frac{Lt}{1+H^q t^q}, \quad (36)$$

$$0 = \frac{2\eta_{ou34} - 2\phi_{ou34} \frac{g}{h} + \delta_{ou34} \frac{g^2}{h^2}}{E_F e^{\frac{g}{2h} \left(\frac{h_2}{2}, \frac{h_3}{2} \right)}} + \left[(n-1) \delta_{ou34}^{n-2} \phi_{ou34}^2 + 2\delta_{ou34}^{n-1} \eta_{ou34} \right] \frac{nLt}{1+H^q t^q}, \quad (37)$$

$$N_3 = \delta_{ou34} b(h_2 + h_3) + \frac{1}{12} \eta_{ou34} b(h_2 + h_3)^3, \quad (38)$$

$$M_3 = \frac{1}{12} \phi_{ou34} b h_3^3, \quad (39)$$

where ε_{ctou34} is the strain in the centre of the cross-section of outer part of portion, D_3D_4 , of the arch, N_3 and M_3 are, respectively, the axial force and the bending moment (it is obvious that $N_3 = 0$), δ_{ou34} , ϕ_{ou34} and η_{ou34} are the coefficients in the series of Maclaurin. The bending moment, M_3 , in the outer part of portion, D_3D_4 , of the arch is written as (Fig. 1)

$$M_3 = M. \quad (40)$$

Eqs. (35)-(39) are solved with respect to ε_{ctou34} , κ_2 , δ_{ou34} , ϕ_{ou34} and η_{ou34} by using the MatLab computer program.

The complementary strain energies, U_{ou}^* and U_{ou34}^* , are expressed as

$$U_{ou}^* = a_2 \iint_{(A_2)} u_{0ou}^* dA, \quad (41)$$

$$U_{ou34}^* = (a_1 - a_2) \iint_{(A_3)} u_{0ou34}^* dA, \quad (42)$$

where A_2 and A_3 are the areas of the cross-sections of the outer parts of portion, D_2D_3 , of the arch and the area of the outer part of portion, D_3D_4 , of the arch, respectively.

Eqs. (17)-(28) are solved with respect to M_1 , κ_1 , ε_{ct} , δ , φ , η , M_2 , ε_{ctou} , κ_4 , δ_{ou} , ϕ_{ou} and η_{ou} by using the MatLab computer program.

The strain energy, U , that is involved in (7) is written as

$$U = U_{md} + U_{ou} + U_{ou34} + U_{unc}, \quad (43)$$

where U_{md}^* , U_{ou} , U_{ou34} and U_{unc} are the strain energies in half of the middle and in half of the outer parts of portion, D_2D_3 , of the arch, in the outer part of portion, D_3D_4 , of the arch, and in the un-cracked portion, B_2P , of the arch, respectively. It should be noted here that the strain energy in the inner part of portion, D_1D_4 , of the arch is zero since this part is free of stresses (Fig. 1).

The strain energies, U_{md} , U_{ou} , U_{ou34} , are obtained by applying formulae (30), (41) and (42), respectively. For this purpose, u_{0md}^* , u_{0ou}^* and u_{0ou34}^* are replaced by the strain energy densities, u_{0md} , u_{0ou} and u_{0ou34} , respectively. The strain energy density, u_{0md} , is calculated by (33). The strain energy densities, u_{0ou} and u_{0ou34} , are found by replacing of σ with σ_{ou} and σ_{ou34} in (33). The strain energy in the un-cracked portion of the arch is expressed as

$$U_{unc} = (s_l - a_1) \iint_{(A_4)} u_{0unc} dA, \quad (44)$$

where A_4 is the area of the cross-section of the arch. The strain energy density, u_{0unc} , is found by replacing of σ with σ_{unc} in (33). The normal stress, σ_{unc} , in the un-cracked portion of the arch is expanded in series of Maclaurin. The coefficients of the series are obtained from the following equations

$$\varepsilon_{ctunc} = \frac{\delta_{unc}}{E_F e^{\frac{g}{2}}} + \delta_{unc}^n \frac{Lt}{1 + H^q t^q}, \quad (45)$$

$$\kappa_3 = \frac{\phi_{unc} - \frac{\delta_{unc} g}{h}}{E_F e^{\frac{g}{2}}} + n \delta_{unc}^{n-1} \phi_{unc} \frac{Lt}{1 + H^q t^q}, \quad (46)$$

$$0 = \frac{2\eta_{unc} - 2\phi_{unc} \frac{g}{h} + \delta_{unc} \frac{g^2}{h^2}}{E_F e^{\frac{g}{2}}} + \left[(n-1) \delta_{unc}^{n-2} \phi_{unc}^2 + 2\delta_{unc}^{n-1} \eta_{unc} \right] \frac{nLt}{1 + H^q t^q}, \quad (47)$$

$$N_4 = \delta_{unc} bh + \frac{1}{12} \eta_{unc} bh^3, \quad (48)$$

$$M = \frac{1}{12} \phi_{unc} bh^3, \quad (49)$$

where ε_{ctunc} is the strain in the centre of the cross-section of the un-cracked portion of the arch, N_4 is the axial force (obviously, $N_4 = 0$), δ_{unc} , ϕ_{unc} and η_{unc} are the coefficients in the series of Maclaurin. Eqs. (45)-(49) are solved with respect to ε_{ctunc} , κ_3 , δ_{unc} , ϕ_{unc} and η_{unc} by using the MatLab computer program.

By substituting of ϕ and U in (7), one derives the following solution to the strain energy release rate at increase of the length of crack, $B_1 B_2$

$$G = 2 \left[\frac{M}{b} \left(\kappa_2 - \kappa_3 \right) - \frac{1}{b} \left(\iint_{(A_3)} u_{0ou34} dA - \iint_{(A_4)} u_{0unc} dA \right) \right]. \quad (50)$$

The integration in (50) is carried-out by using the MatLab computer program.

A solution to the strain energy release rate is obtained also at increase of the length of crack, $C_1 C_2$. For this purpose, (7) is re-written as

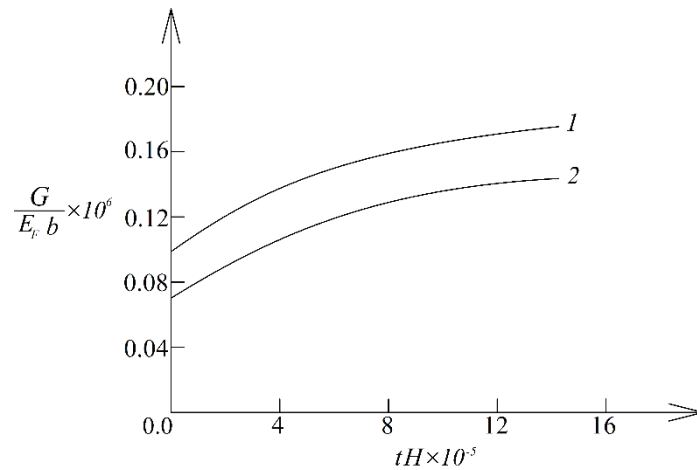


Fig. 3 The strain energy release rate in non-dimensional form plotted against the non-dimensional time (curve 1 - at increase of crack, $B_1 B_2$, curve 2 - at increase of crack, $C_1 C_2$)

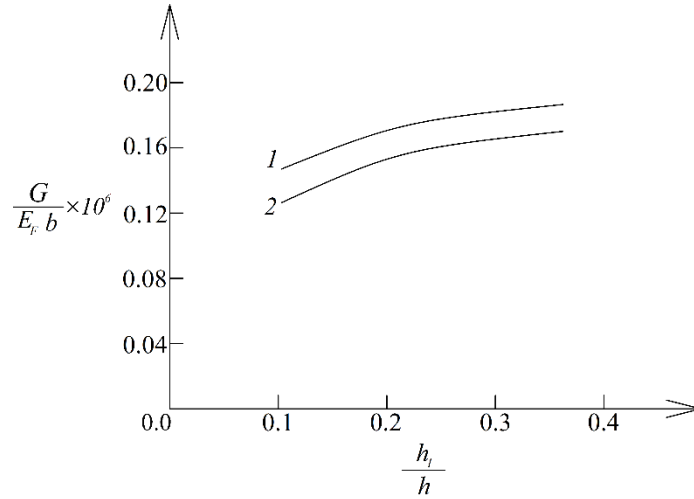


Fig. 4. The strain energy release rate in non-dimensional form plotted against h_1/h ratio (curve 1 - at increase of crack, B_1B_2 , curve 2 - at increase of crack, C_1C_2)

$$G = 2 \left(\frac{M}{b} \frac{\partial \phi}{\partial a_2} - \frac{1}{b} \frac{\partial U}{\partial a_2} \right). \quad (51)$$

By substituting of ϕ and U in (51), one derives

$$G = 2 \left[\frac{M}{b} (\kappa_1 - \kappa_2) - \frac{1}{b} \left(\iint_{(A_1)} u_{0md}^* dA + \iint_{(A_2)} u_{0ou}^* dA - \iint_{(A_3)} u_{0ou34}^* dA \right) \right]. \quad (52)$$

The MatLab computer program is used to carry-out the integration in (52).

It should be mentioned that solutions (50) and (52) are time-dependent sine the strain energy densities and the changes of the curvatures are functions of time. Therefore, the solutions can be applied to calculate the strain energy release rate for any particular time.

In order to verify (50) and (52), the time-dependent strain energy release rate is obtained also by differentiating the complementary strain energy with respect to the crack area (Rizov 2020). First, an elementary increase, da_1 , of the length of crack, B_1B_2 , is assumed and the strain energy release rate is written as

$$G = 2 \frac{dU^*}{b da_1}. \quad (53)$$

The right-hand of (53) is doubled in view of the symmetry. The complementary strain energy, U^* , is found by (43). For this purpose, U_{md} , U_{ou} , U_{ou34} and U_{unc} are replaced, respectively, with U_{md}^* , U_{ou}^* , U_{ou34}^* and U_{unc}^* .

The complementary strain energy in the un-cracked portion of the arch is obtained by replacing of u_{0unc} with the complementary strain energy density, u_{0unc}^* . Formula (34) is used to calculate u_{0unc}^* . For this purpose, σ is replaced with σ_{unc} . By substituting of the strain energy in (53), one obtains

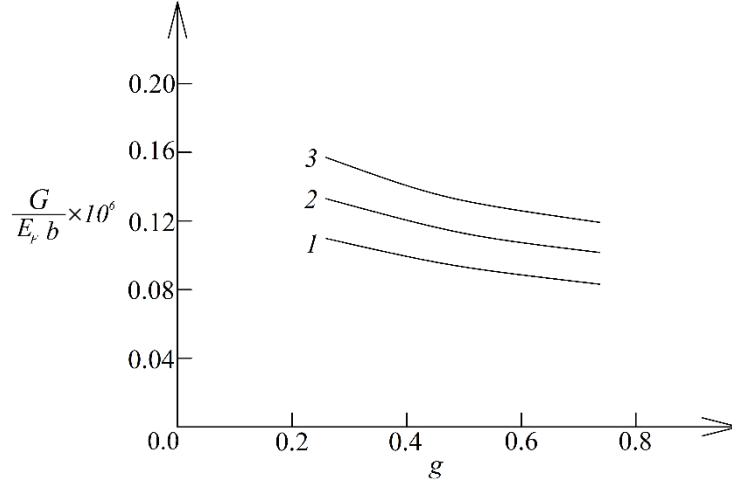


Fig. 5 The strain energy release rate in non-dimensional form plotted against g (curve 1 - at $h_2/h = 0.3$, curve 2 - at $h_2/h = 0.4$ and curve 3 - at $h_2/h = 0.5$)

$$G = \frac{2}{b} \left(\iint_{(A_3)} u_{0ou34}^* dA - \iint_{(A_4)} u_{0unc} dA \right). \quad (54)$$

The integration in (54) is performed by using the MatLab computer program. It should be noted that the strain energy release rate found by (54) is exact match of that obtained by (51). This fact verifies the solution to the strain energy release rate at increase of crack, $B_1 B_2$.

The strain energy release rate is derived also assuming an elementary increase of the length of crack, $C_1 C_2$. By replacing of da_1 with da_2 and substituting of U in (53), one derives

$$G = \frac{2}{b} \left(\iint_{(A_1)} u_{0md}^* dA + \iint_{(A_2)} u_{0ou}^* dA - \iint_{(A_3)} u_{0ou34}^* dA \right). \quad (55)$$

MatLab is used to perform the integration in (55). The fact that the strain energy release rate found by (55) is exact match of that calculated by (52) verifies the solution to the strain energy release rate at increase of crack, $C_1 C_2$.

It should be noted that the strain energy release rate is derived also be retaining more than three members in the series of Maclaurin. The results obtained are very close to these found by retaining the first three members the series of Maclaurin (the difference is less than 1%).

3. Numerical results

In this section of the paper, results which illustrate the influence of the time, material inhomogeneity and the locations of the two longitudinal cracks in the thickness direction on the strain energy release rate in the arch structure are presented. It is assumed that $b = 0.010$ m, $h = 0.014$ m, $q = 0.3$ and $M = 10$ Nm.

Solutions (50) and (52) are applied in order to investigate the evolution of the strain energy release rate with the time. For this purpose, calculations are carried-out for various values of the

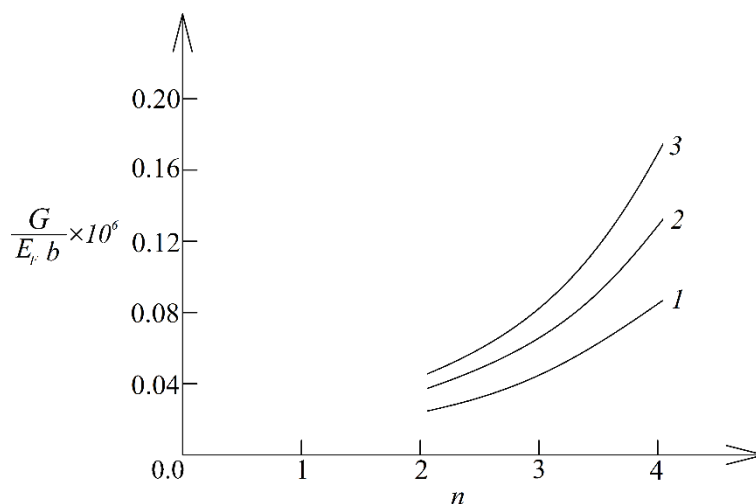


Fig. 6 The strain energy release rate in non-dimensional form plotted against n (curve 1 - at $M = 6$ Nm, curve 2 - at $M = 8$ Nm and curve 3 - at $M = 10$ Nm)

time. The calculated strain energy release rate is expressed in non-dimensional form by using the formula $G_N = G/(E_F b)$. The evolution of the strain energy release rate with the time is illustrated in Fig. 3 where strain energy release rate in non-dimensional form is plotted against the non-dimensional time. It should be noted that the time is expressed in non-dimensional form by using the formula $t_N = tH$. It is evident from Fig. 3 that the strain energy release rate increases with the time (this funding is attributed to the non-linear creep). One can observe also in Fig. 3 that the strain energy release rate obtained at increase of crack, $B_1 B_2$, is higher in comparison with that found at increase of crack, $C_1 C_2$.

The influence of the location of crack, $B_1 B_2$, in the thickness direction on the strain energy release rate is analyzed. The location of crack, $B_1 B_2$, in the thickness direction is characterized by h_1/h ratio. One can get an idea about the influence of the location of crack, $B_1 B_2$, in the thickness direction from Fig. 4 where the strain energy release rate in non-dimensional form is plotted against h_1/h ratio by using solutions (50) and (52). The curves in Fig. 4 indicate that the strain energy release rate increases with increasing of h_1/h ratio.

The effect of the material inhomogeneity and the location of crack, $C_1 C_2$, in the thickness direction on the strain energy release rate is studied too. The location of crack, $C_1 C_2$, is characterized by h_2/h ratio. The material inhomogeneity in the thickness direction is characterized by g . The variation of the strain energy release rate in non-dimensional form with g at three h_2/h ratios is depicted in Fig. 5 by applying the solution to the strain energy release rate derived at increase of crack, $C_1 C_2$. It can be observed in Fig. 5 that the strain energy release rate decreases with increasing of g . The increase of h_2/h ratio leads to increase of the strain energy release rate (Fig. 5).

The change of the strain energy release rate with increasing of n is investigated. For this purpose, calculations of the strain energy release rate are performed at various values of n . The solution to the strain energy release rate derived at increase of the length of crack, $B_1 B_2$, is used. The results obtained are shown in Fig. 6 where the strain energy release rate in non-dimensional form is plotted against n at three values of the bending moment, M . The curves in Fig. 6 show that

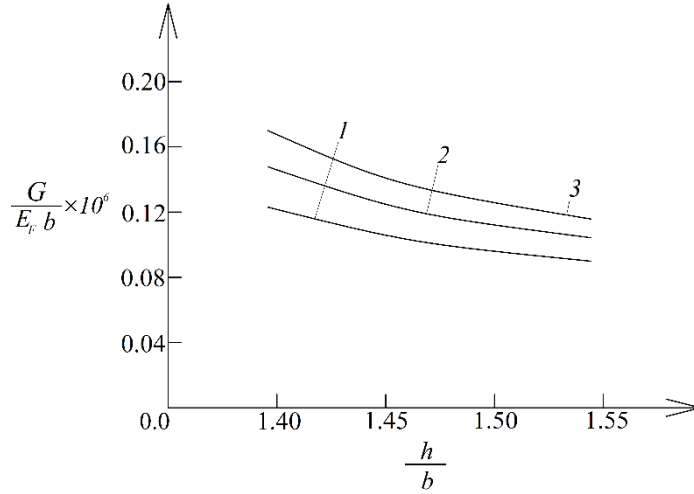


Fig. 7 The strain energy release rate in non-dimensional form plotted against h/b ratio (curve 1 - at $h_3/h = 0.2$, curve 2 - at $h_3/h = 0.3$, curve 3 - at $h_3/h = 0.4$)

the strain energy release rate increases with increasing of n .

The variation of the strain energy release rate with increasing of h/b ratio at three h_3/h ratios is depicted in Fig. 7. The solution obtained at increase of the length of crack, B_1B_2 , is applied.

It is evident from Fig. 7 that the strain energy release rate decreases with increasing of h/g ratio. Concerning the influence of h_3/h ratio, the curves in Fig. 7 indicate that the strain energy release rate increases with increasing of h_3/h ratio.

5. Conclusions

The fracture of an inhomogeneous arch structure with two longitudinal cracks subjected to non-linear creep is studied. For this purpose, time-dependent solutions to the strain energy release rate are derived by analyzing the balance of the energy. The mechanical behavior of the material is described by using a non-linear stress-strain-time relationship. The arch under consideration has a rectangular cross-section. The material exhibits continuous inhomogeneity along the thickness of the cross-section of the arch. The two longitudinal cracks are located symmetrically with respect to the mid-span. In the thickness direction, the arch is divided in inner, middle and outer parts by the two cracks. The arch is loaded by two bending moments applied at the end sections. For verification, the time-dependent strain energy release rate is derived also by considering the time-dependent complementary strain energy. The evolution of the strain energy release rate with the time is studied. It is found that the strain energy release rate increases with time due to the non-linear creep behavior of the material. The study indicates also that the strain energy release rate obtained at increase of the inner crack is higher than that found at increase of the outer crack. The analysis reveals that the strain energy release rate increases with increasing of h_1/h , h_2/h and ratios h_3/h . The calculations indicate that the increase of g leads to decrease of the strain energy release rate. It is found that the strain energy release rate increases with increasing of n . The increase of h/b ratio causes decrease of the strain energy release rate.

Acknowledgments

The financial support provided by the German Academic Exchange Organization (DAAD) for the research stay of the first author (V.I.R.) in Department of Engineering Mechanics, Institute of Mechanics, Otto-von-Guericke-University, Magdeburg, Germany is gratefully acknowledged.

References

- Ahmed, R.A., Fenjan, R.M., Hamad, L.B. and Faleh, N.M. (2020), "A review of effects of partial dynamic loading on dynamic response of nonlocal functionally graded material beams", *Adv. Mater. Res.*, **9**(1), 33-48. <https://doi.org/10.12989/amr.2020.9.1.033>.
- Altunsaray, E. (2017), "Static deflections of symmetrically laminated quasi-isotropic super-elliptical thin plates", *Ocean Eng.*, **141**, 337-350. <https://doi.org/10.1016/j.oceaneng.2017.06.032>.
- Altunsaray, E. and Bayer, İ. (2014), "Buckling of symmetrically laminated quasi-isotropic thin rectangular plates", *Steel Compos. Struct.*, **17**, 305-320. <https://doi.org/10.12989/scs.2014.17.3.305>.
- Altunsaray, E., Ünsalan, D., Neşer, G., Gürsel, K.T. and Taner, M. (2019), "Parametric study for static deflections of symmetrically laminated rectangular thin plates", *Scientif. Bull. Mircea cel Batran Naval Academy*, **22**, 1-12. <https://doi.org/10.21279/1454-864X-19-11-041>.
- Avcar, M. and Mohammed, W.K.M. (2018), "Free vibration of functionally graded beams resting on Winkler-Pasternak foundation", *Arab. J. Geosci.*, **11**, 232. <https://doi.org/10.1007/s12517-018-3579-2>.
- Butcher, R.J., Rousseau, C.E. and Tippur, H.V. (1999), "A functionally graded particulate composite: Measurements and failure analysis", *Acta. Mater.*, **47**(2), 259-268. [https://doi.org/10.1016/S1359-6454\(98\)00305-X](https://doi.org/10.1016/S1359-6454(98)00305-X).
- Dolgov, N.A. (2005), "Determination of stresses in a two-layer coating", *Strength Mater.*, **37**(2), 422-431. <https://doi.org/10.1007/s11223-005-0053-7>.
- Dolgov, N.A. (2016), "Analytical methods to determine the stress state in the substrate-coating system under mechanical loads", *Strength Mater.*, **48**(1), 658-667. <https://doi.org/10.1007/s11223-016-9809-5>.
- Gasik, M.M. (2010), "Functionally graded materials: bulk processing techniques", *Int. J. Mater. Prod. Technol.*, **39**(1-2), 20-29. <https://doi.org/10.1504/IJMPT.2010.034257>.
- Hedia, H.S., Aldousari, S.M., Abdellatif, A.K. and Fouda, N.A. (2014), "New design of cemented stem using functionally graded materials (FGM)", *Biomed. Mater. Eng.*, **24**(3), 1575-1588. <https://doi.org/10.3233/BME-140962>.
- Hirai, T. and Chen, L. (1999), "Recent and prospective development of functionally graded materials in Japan", *Mater. Sci. Forum*, **308-311**(4), 509-514. <https://doi.org/10.4028/www.scientific.net/MSF.308-311.509>.
- Kishkilov, M. and Apostolov, R. (1994), *Introduction to Theory of Plasticity*, UACEG.
- Madan, R., Saha, K. and Bhowmick, S. (2020), "Limit speeds and stresses in power law functionally graded rotating disks", *Adv. Mater. Res.*, **9**(2), 115-131. <https://doi.org/10.12989/amr.2020.9.2.115>.
- Mahamood, R.M. and Akinlabi, E.T. (2017), *Functionally Graded Materials*, Springer.
- Markworth, A.J., Ramesh, K.S. and Parks, Jr. W.P. (1995), "Review: Modeling studies applied to functionally graded materials", *J. Mater. Sci.*, **30**(3), 2183-2193. <https://doi.org/10.1007/BF01184560>.
- Miyamoto, Y., Kaysser, W.A., Rabin, B.H., Kawasaki, A. and Ford, R.G. (1999), *Functionally Graded Materials: Design, Processing and Applications*, Kluwer Academic Publishers, Dordrecht/London/Boston.
- Nemat-Allal, M.M., Ata, M.H., Bayoumi, M.R. and Khair-Eldeen, W. (2011), "Powder metallurgical fabrication and microstructural investigations of Aluminum/Steel functionally graded material", *Mater. Sci. Appl.*, **2**(5), 1708-1718. <https://doi.org/10.4236/msa.2011.212228>.
- Rabenda, M. (2015), "Analysis of non-stationary heat transfer in a hollow cylinder with functionally graded material properties performed by different research methods", *Eng. Trans.*, **63**, 329-339.

- Rabenda, M. (2016), "The analysis of the impact of different shape functions in tolerance modeling on natural vibrations of the rectangular plate with dense system of the ribs in two directions", *Vib. Phys. Syst.*, **27**, 301-308.
- Rabenda, M. and Michalak, B. (2015), "Natural vibrations of prestressed thin functionally graded plates with dense system of ribs in two directions", *Compos. Struct.*, **133**, 1016-1023. <https://doi.org/10.1016/j.compstruct.2015.08.026>.
- Rizov, V. and Altenbach, H. (2020), "Longitudinal fracture analysis of inhomogeneous beams with continuously varying sizes of the cross-section along the beam length", *Frattura ed Integrità Strutturale*, **53**, 38-50. <https://doi.org/10.3221/IGF-ESIS.53.04>.
- Rizov, V.I. (2020), "Longitudinal fracture analysis of inhomogeneous beams with continuously changing radius of cross-section along the beam length", *Strength Fract. Complex.*, **13**, 31-43. <https://doi.org/10.3233/SFC-200250>.
- Rizov, V.I. (2020a), "Inhomogeneous multilayered beams of linearly changing width: a delamination analysis", *IOP Conf. Ser.: Mater. Sci. Eng.*, **739**, 012004. <https://doi.org/10.1088/1757-899X/739/1/012004>.
- Rizov, V.I. (2022), "Analysis of the strain energy release rate for time-dependent delamination in multilayered beams with creep", *Adv. Mater. Res.*, **11**, 41-57. <https://doi.org/10.12989/amr.2022.11.1.041>.
- Saiyathibrahim, A., Subramaniyan, R. and Dhanapl, P. (2016), "Centrifugally cast functionally graded materials-review", *International Conference on Systems, Science, Control, Communications, Engineering and Technology*, 68-73.
- Shrikantha Rao, S. and Gangadharan, K.V. (2014), "Functionally graded composite materials: an overview", *Procedia Mater. Sci.*, **5**(1), 1291-1299. <https://doi.org/10.1016/j.mspro.2014.07.442>.
- Sofiyev, A.H., Alizada, A.N., Akin, Ö., Valiyev, A., Avcar, M. and Adiguzel, S. (2012), "On the stability of FGM shells subjected to combined loads with different edge conditions and resting on elastic foundations", *Acta Mech.*, **223**, 189-204. <https://doi.org/10.1007/s00707-011-0548-1>.
- Sofiyev, A.H. and Avcar, M. (2010), "The stability of cylindrical shells containing an FGM layer subjected to axial load on the Pasternak foundation", *Eng.*, **2**, 228-236 <https://doi.org/10.4236/eng.2010.24033>.
- Uslu Uysal, M. (2016), "Buckling behaviours of functionally graded polymeric thin-walled hemispherical shells", *Steel Compos. Struct.*, **21**(1), 849-862. <https://doi.org/10.12989/scs.2016.21.4.849>.
- Uslu Uysal, M. and Güven, U. (2015), "Buckling of functional graded polymeric sandwich panel under different load cases", *Compos. Struct.*, **121**, 182-196. <https://doi.org/10.1016/j.compstruct.2014.11.012>.
- Uslu Uysal, M. and Güven, U. (2016), "A bonded plate having orthotropic inclusion in adhesive layer under in-plane shear loading", *J. Adhes.*, **92**, 214-235. <https://doi.org/10.1080/00218464.2015.1019064>.
- Uslu Uysal, M. and Kremzer, M. (2015), "Buckling behaviour of short cylindrical functionally gradient polymeric materials", *Acta Physica Polonica*, **A127**, 1355-1357. <https://doi.org/10.12693/APhysPolA.127.1355>.
- Wu, X.L., Jiang, P., Chen, L., Zhang, J.F., Yuan, F.P. and Zhu, Y.T. (2014), "Synergetic strengthening by gradient structure", *Mater. Res. Lett.*, **2**(1), 185-191. <https://doi.org/10.1080/21663831.2014.935821>.